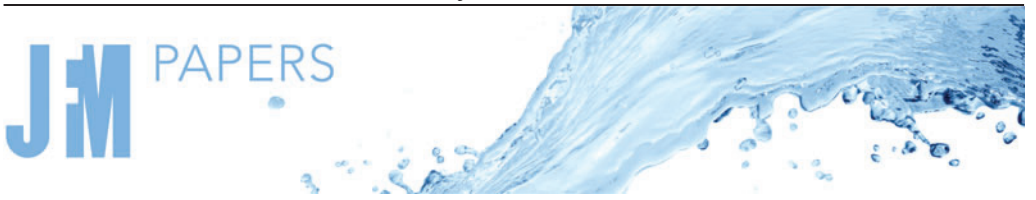
J. Fluid Mech. (2022), *vol*. 940, A25, doi:10.1017/jfm.2022.242



A new equivalent sand grain roughness relation for two-dimensional rough wall turbulent boundary layers

Misarah Abdelaziz[1],†, L. Djenidi[2], Mergen H. Ghayesh[1] and Rey Chin[1]

[1]School of Mechanical Engineering, University of Adelaide, Adelaide, South Australia 5005, Australia

[2]Mechanical Engineering Discipline, The University of Newcastle, Callaghan, NSW 2308, Australia

(Received 18 April 2021; revised 8 February 2022; accepted 13 March 2022)

The effects of different geometries of two-dimensional (2-D) roughness elements in a zero pressure gradient (ZPG) turbulent boundary layer (TBL) on turbulence statistics and drag coefficient are assessed using single hot-wire anemometry. Three kinds of 2-D roughness are used: (i) circular rods with two different heights, $k = 1.6$ and 2.4 mm, and five different streamwise spacing of $s_x = 6k$ to $24k$, (ii) three-dimensional (3-D) printed triangular ribs with heights of $k = 1.6$ mm and spacing of $s_x = 8k$ and (iii) computerized numerical control (CNC) machined sinewave surfaces with two different heights, $k = 1.6$ and 2.4 mm, and spacing of $s_x = 8k$. These roughnesses cover a wide range of ratios of the boundary layer thickness to the roughness height ($23 < \delta/k < 41$), where δ is the boundary layer thickness. All roughnesses cause a downward shift on the wall-unit normalised streamwise mean velocity profile when compared with the smooth wall profiles agreeing with the literature, with a maximum downward shift observed for $s_x = 8k$. In the fully rough regime, the drag coefficient becomes independent of the Reynolds number. Changing the roughness height while maintaining the same spacing ratio s_x/k exhibits little influence on the drag coefficient in the fully rough regime. On the other hand, the effective slope (ES) and the height skewness (k_{sk}) appear to be major surface roughness parameters that affect the drag coefficient. These parameters are used in a new expression for k_s, the equivalent sand grain roughness, developed for 2-D uniformly distributed roughness in the fully rough regime.

Key words: turbulent boundary layers

1. Introduction

Turbulence is arguably one of the most difficult subjects in nonlinear physics due to its complex and challenging mathematical descriptions, its inherent instabilities and chaotic

† Email address for correspondence: misarah.abdelaziz@adelaide.edu.au

© The Author(s), 2022. Published by Cambridge University Press

https://doi.org/10.1017/jfm.2022.242 Published online by Cambridge University Press

nature (Sun 2019). The presence of a wall compounds further the challenge to investigate turbulence, such as in turbulent boundary layers. In addition, complications arise when the wall is rough.

Rough wall flows tend to produce a higher coefficient of friction ($C_f = 2\tau_w/\rho U_\infty^2$, where U_∞ is the free-stream velocity, τ_w is the wall shear stress and ρ is the density of the fluid), than flows over smooth surfaces. The increase of C_f is manifested in the downward shift of the wall–unit normalised mean velocity profile when compared with the smooth wall profile (Hama 1954). The shift, known as the roughness function, is defined as $\Delta U^+ = \Delta U/U_\tau$, where U is the mean streamwise velocity and U_τ is the friction velocity $U_\tau = \sqrt{\tau_w/\rho}$; the superscript, $(^+)$ means normalisation by the wall units U_τ or ν/U_τ, where ν is the kinematic viscosity. The roughness function is a function of the equivalent sand grain roughness k_s (Schlichting & Kestin 1961). Ideally, one would like to determine ΔU^+ based solely on the roughness topology. This would provide a way of predicting C_f without the need to perform lengthy measurements. Unfortunately, k_s is not a physical roughness parameter and its determination relies on an empirical method based on the mean velocity profile (Nikuradse 1933).

When k_s^+ is large enough the flow is considered to be in the 'fully rough' regime and the drag is mainly composed of the pressure (or form) drag (Squire *et al.* 2016). This regime is characterised by a log–linear relationship between ΔU^+ and k_s^+. On the other hand, when k_s^+ is too small, the roughness does not have a noticeable effect on the viscous sublayer of the flow. This flow regime is called 'dynamically smooth' and can be treated as a smooth wall flow. At moderate values of k_s^+, both the pressure drag and the viscous drag contribute to the total drag. This flow regime is called 'transitionally rough' (Nikuradse 1933). So far there are no clear thresholds that delimit these flow regimes. However, it is commonly agreed that the flow is hydraulically smooth when $k_s^+ < 4$, and fully rough when $k_s^+ > 70$ (Jiménez 2004).

The roughness function ΔU^+ is determined by 'measuring' the vertical shift between the log regions of the rough wall and smooth wall wall-unit normalised velocity profiles. This requires that experiments be conducted for each rough surface to obtain the velocity profile and friction velocity. A more practical way to proceed, but one that also presents a big challenge, is to predict ΔU^+ directly from surface topology or by other means, correlating k_s to one or more parameters characterising the roughness. So far, there has been no definite consensus on which length scale or roughness parameter best characterises a surface that can correlate with the friction drag. Over the last decade, a large body of work has been undertaken to address this issue (Musker 1980; Napoli, Armenio & De Marchis 2008; Schultz & Flack 2009; Forooghi *et al.* 2017; Flack, Schultz & Barros 2020, among many others). A wide range of different surface parameters has been studied to predict which of these parameters dominantly affects the friction drag. Some of these parameters are the mean roughness height k_a, root-mean-square height k_{rms}, maximum peak to valley height k, average peak to valley height k_z, effective slope ES, solidarity λ_f, skewness k_{sk} and flatness k_{ku}. However, none of these parameters is sufficient to be generalised for all kinds of roughness.

Musker (1980) developed a modified roughness Reynolds number as a function of simple geometric statistics (average absolute slope, standard deviation, skewness and flatness) for naturally occurring surfaces as follows:

$$k_s^+ = \frac{\sigma U_\tau}{\nu}(1 + aES)(1 + bk_{sk}k_{ku}), \tag{1.1}$$

https://doi.org/10.1017/jfm.2022.242 Published online by Cambridge University Press

where a and b are constants to give the best fit of roughness functions related to naturally occurring surfaces, and σ is the standard deviation of the surface roughness.

Waigh & Kind (1998) studied a regular three-dimensional (3-D) roughness and found that the element bluntness and spanwise aspect ratio are the main parameters characterising the roughness function as follows:

$$\Delta U^+ = \begin{cases} 10.56 \log\left[\left(\dfrac{1}{\lambda_f}\dfrac{k}{b_m}\right)^{0.87}\left(\dfrac{A_w}{A_f}\right)^{0.44}\right] - 7.59 & \Lambda < 6, \\ -5.57 \log\left[\left(\dfrac{1}{\lambda_f}\dfrac{k}{b_m}\right)^{0.55}\left(\dfrac{A_w}{A_f}\right)^{1.38}\right] + 5.78 & \Lambda > 6, \end{cases} \tag{1.2}$$

where $\Lambda = \lambda_f k/s_m$, s_m is the streamwise width of the roughness element, b_m is the spanwise width of the roughness element, $\lambda_f = A_f/A_s$, A_s is the surface area, A_f is the projected frontal area and A_w is the wetted area.

Bons (2002) derived a new k_s correlation, based on the surface slope angle for real turbine roughness; the roughness panels were scaled models of actual turbine surfaces instead of using the traditional simulated roughness

$$k_s = -0.0261ES + 0.0138ES^2. \tag{1.3}$$

Schultz & Flack (2009) studied close-packed pyramid roughnesses to study the effect of the height and slope of roughness on the flow. They found that ΔU^+ mainly depends on the roughness height. They also found a range of ES such that, below this level, the surface is considered to be wavy, not rough, and the roughness function strongly depends on the ES. If $ES < 0.35$, the surface is considered to be wavy.

Forooghi *et al.* (2017) investigated numerically the effect of various roughness parameters on k_s in the fully rough regime of channel flow at friction Reynolds number $Re_\tau \approx 500$. Their roughness geometries were generated by systematically changing the moments of the surface height probability density function, the effective slope of the random roughness and the size distribution of the roughness peaks. Forooghi *et al.* (2017) correlate k_s based on k, k_{sk} and Es. They found that these roughness parameters can predict k_s accurately for randomly distributed roughness in the fully rough regime of channel flows

$$\left.\begin{aligned} k_s/k &= F(k_{sk})G(ES), \\ F(k_{sk}) &= 0.67k_{sk}^2 + 0.93k_{sk} + 1.3, \\ G(ES) &= 1.07(1 - \mathrm{e}^{-3.5ES}). \end{aligned}\right\} \tag{1.4}$$

Flack *et al.* (2020) investigated the importance of roughness height and skewness on the coefficient of friction. A k_s correlation was derived as

$$k_s = A_1 k_{rms}(1 + k_{sk})^{B_1}, \tag{1.5}$$

with $A_1 = 4.43$ and $B_1 = 1.37$.

While many roughness function formulations in terms of one or more roughness parameters have been proposed recently, they are limited to the particular roughness investigated. In other words, they lack universality. This is certainly associated with the fact that, so far, a 'universal' critical parameter for all roughnesses is yet to be determined. Whether such 'universal' parameter exists or not is still an open issue. It is nevertheless conceivable that such parameter can be identified for families of rough surfaces, such

https://doi.org/10.1017/jfm.2022.242 Published online by Cambridge University Press

as 2-D roughness and 3-D roughness, in the fully rough regime. The present work is an attempt to determine such a parameter with the view to develop an expression for k_s. The roughness family considered here is that of 2-D roughness. One reason to focus on this roughness family is that it was shown to produce a fully rough regime at relatively low Reynolds number, which can be easily achieved in wind tunnels. For example the use of 2-D rods attached to a smooth wall where the spacing between two consecutive rods, s_x, is approximately $8k$ leads to a fully rough regime (Djenidi, Talluru & Antonia 2018). In their direct numerical simulations of a turbulent rough wall channel flow, Leonardi *et al.* (2003) used transverse square bars as a roughness, with s_x varying from $2k$ to $32k$. They showed that the form drag was the main contributor to the total drag when $8k \leq s_x \leq 16k$. Later, Leonardi *et al.* (2015) used circular rods and investigated friction and pressure drags numerically, confirming their previous observations. Kamruzzaman *et al.* (2015) investigated the turbulent boundary layer developed over a rod roughened wall that has a spacing between two consecutive rods of $8k$. They calculated the pressure drag directly from the distribution of static pressure around one rod. They revealed that C_f is constant and independent of the Reynolds number in the fully rough regime. This was further confirmed by Djenidi *et al.* (2018).

In this present work, we carry out turbulent boundary layer measurements over various 2-D rough surfaces with a height ratio δ/k ranging from 23 to 41. Two sets of experiments are conducted. The first one is to validate our rough wall measurements and estimation of U_τ. Also, the experiments are used to validate the Reynolds number independence when the flow is fully rough. The second set of experiments is exploited to determine the most critical dominant roughness parameters impacting C_f with the view to developing an expression for k_s^+ valid for the 2-D rough wall family.

2. Experimental details

2.1. *Wind tunnel facility*

The experiments are performed in a closed-return-type wind tunnel located at the University of Adelaide. It can achieve a maximum velocity of 30 m s^{-1} with a low-level turbulence intensity of approximately 0.53 %. The test section is rectangular and has a cross-section of 500 mm × 300 mm and a 2000 mm length. A 125 mm long circulation flap is also installed downstream of the test section to reduce the circulations generated over the flat plates as much as possible and to make sure that the stagnation point is on the measurement side of the plate. This flap can be regulated to keep the flow with a zero pressure gradient (ZPG) along with adjusted sidewalls. The tunnel should be wider than six times the boundary layer thickness to ensure the boundary layer developed in the test section is two-dimensional, as reported by Nickels *et al.* (2005). In our measurements, the 500 mm width is more than 7δ of the largest boundary layer thickness developed. The inlet flow is tripped by a 4 mm diameter rod and a 100 mm strip of sandpaper with a 40 grit number.

2.2. *Surface roughness*

The roughness details of this study are: circular rods of 500 mm length with two different diameters, $k = 1.6$ and 2.4 mm, and five different streamwise spacing ratios s_x/k ranges from 6 to 24. A total of 30 plates, 3-D printed triangular ribs, of $k = 1.6$ mm and $8k$ spacing; each plate measures 145 mm × 153.6 mm. The 3D printed triangular ribs were printed from acrylonitrile butadiene styrene (ABS) plastic material using a fused

https://doi.org/10.1017/jfm.2022.242 Published online by Cambridge University Press

deposition modelling 3D printer, Zortrax M200. This model has an accuracy of 200 μm in the x and z directions, and a layer height of 90 μm with a 0.4 mm nozzle diameter, where x and z are the streamwise and spanwise directions, respectively. A total of 8 CNC machined plates are employed, each of which has a 2-D sinewave surface function, an amplitude of $k/2 = 0.8$ mm and a wavelength of $8k$; each plate measures 435 mm × 192 mm. These CNC machined surfaces were machined by a custom carbide engraving cutter of a TORMACH PCNC-series 3 machine. Two CNC machined plates have a 2-D sinewave surface function, an amplitude of $k/2 = 1.2$ mm and a wavelength of $8k$; each plate measures 480 mm × 768 mm. This surface was fabricated by a Multicam M1212 Router machine, with a 0.6 mm stepover and 12 mm ball nose cutter. The absolute values of the profile heights for different rough surfaces are described as follows: a periodic function describes the rough surface of the circular rods, triangular ribs and sinewaves, respectively, as follows:

$$Z(x) = \begin{cases} \sqrt{kx - x^2} & 0 \le x \le k, \\ \dfrac{-k}{2} & k < x < s_x, \end{cases} \tag{2.1}$$

$$Z(x) = \begin{cases} \dfrac{-k}{2} + \dfrac{2kx}{s_x} & 0 \le x \le s_x/2, \\ \dfrac{-k}{2} + \dfrac{2k(s_x - x)}{s_x} & s_x/2 \le x \le s_x, \end{cases} \tag{2.2}$$

$$Z(x) = \frac{k}{2} \sin\left(\frac{2\pi x}{s_x}\right), \tag{2.3}$$

where $k = 1.6$ mm and $s_x = 8k$. The surfaces are defined by the first letter of the shape name: R for rods, T for triangular ribs and S for sinewaves followed by $10k$ and finally the spacing ratio between two consecutive roughness peaks. For example $R16-08$ means a surface with cylindrical rods with a height of 1.6 mm and spacing ratio between two consecutive roughness rods of 8. All different roughnesses, as well as the strip of sandpaper are taped using double-sided tape on an aluminium sheet of dimensions 500mm × 1600 mm. Statistical parameters used to characterise the different rough surfaces are tabulated in table 1.

The roughness average height k_a, is defined by ASME (2009) as the arithmetic average of the absolute values of the profile height deviations from the mean m line, defined on the sampling length L_s as

$$k_a = \frac{1}{L_s} \int_0^{L_s} |Z(x) - m| \, \mathrm{d}x. \tag{2.4}$$

The root-mean-square height k_{rms} corresponds to the standard deviation σ of the height distribution, defined on the sampling length as

$$k_{rms} = \sqrt{\frac{1}{L_s} \int_0^{L_s} Z(x)^2 \, \mathrm{d}x}. \tag{2.5}$$

The roughness skewness k_{sk} (normalised third-order moment), is the asymmetry of the height distribution, defined on the sampling length. This parameter is crucial, as it indicates a morphology of the surface texture (see Flack *et al.* 2016). Positive values correspond to high peaks spread on a regular surface, while negative values correspond to

https://doi.org/10.1017/jfm.2022.242 Published online by Cambridge University Press

No.	Surface	k (mm)	s_x (mm)	k_a (mm)	k_{rms} (mm)	k_{sk}	k_{ku}	ES	λ_f
01	$R16-06$	1.6	9.60	0.40	0.59	1.85	4.53	0.333	0.1670
02	$R16-08$	1.6	12.8	0.31	0.51	2.34	6.57	0.250	0.1250
03	$R16-12$	1.6	19.2	0.22	0.42	3.09	10.7	0.167	0.0830
04	$R16-16$	1.6	25.6	0.17	0.36	3.70	14.9	0.125	0.0625
05	$R16-24$	1.6	38.4	0.11	0.29	4.69	23.3	0.083	0.0417
06	$R24-06$	2.4	14.4	0.60	0.88	1.85	4.53	0.333	0.1670
07	$R24-08$	2.4	19.2	0.47	0.76	2.34	6.57	0.250	0.1250
08	$R24-12$	2.4	28.8	0.33	0.62	3.09	10.7	0.167	0.0830
09	$R24-16$	2.4	38.4	0.25	0.54	3.70	14.9	0.125	0.0625
10	$R24-24$	2.4	57.6	0.17	0.44	4.69	23.3	0.083	0.0417
11	$T16-08$	1.6	12.8	0.40	0.92	0.00	1.80	0.250	0.1250
12	$S16-08$	1.6	12.8	0.51	0.57	0.00	1.50	0.250	0.1250
13	$S24-08$	2.4	19.2	0.76	0.85	0.00	1.50	0.250	0.1250

Table 1. Different key surface roughness parameters.

surfaces with pores and scratches. However, this parameter does not give any information about the absolute height of the profile, contrary to k_a

$$k_{sk} = \frac{1}{\sigma^3 L_s}\int_0^{L_s}(Z(x)-m)^3\,\mathrm{d}x. \tag{2.6}$$

The roughness kurtosis k_{ku} (normalised fourth-order moment), is the sharpness of the height distribution, defined on the sampling length as

$$k_{ku} = \frac{1}{\sigma^4 L_s}\int_0^{L_s}(Z(x)-m)^4\,\mathrm{d}x. \tag{2.7}$$

The equation for the effective slope ES, which is the mean absolute streamwise gradient of the surface, as defined by Napoli *et al.* (2008) for 2-D rough surfaces is as follows:

$$ES = \frac{1}{L_s}\int_0^{L_s}\left|\frac{\mathrm{d}Z(x)}{\mathrm{d}x}\right|\mathrm{d}x, \tag{2.8}$$

this parameter is also related to the solidity λ_f, which is defined as the total projected frontal area of the roughness element A_f per unit wall parallel area A_p, by the relationship $ES = 2\lambda_f$ (see Napoli *et al.* 2008)

$$\lambda_f = \frac{A_f}{A_p}. \tag{2.9}$$

2.3. *Measurement rig*

Single hot-wire probes with 5 μm diameter tungsten wire, and 1 mm sensing length (l) are used in measurements to give a length to diameter ratio of approximately 200, as recommended by Ligrani & Bradshaw (1987) and Hutchins *et al.* (2009). An overheat ratio of 1.6 is applied using an IFA300 constant temperature anemometer. A T-type thermocouple integrated with the IFA300 is used to record the mean temperature in the free stream throughout the experiment. Dynamic calibration of the hot-wire is performed with a square wave test also integrated into the IFA300 to determine the cutoff frequency of

https://doi.org/10.1017/jfm.2022.242 Published online by Cambridge University Press

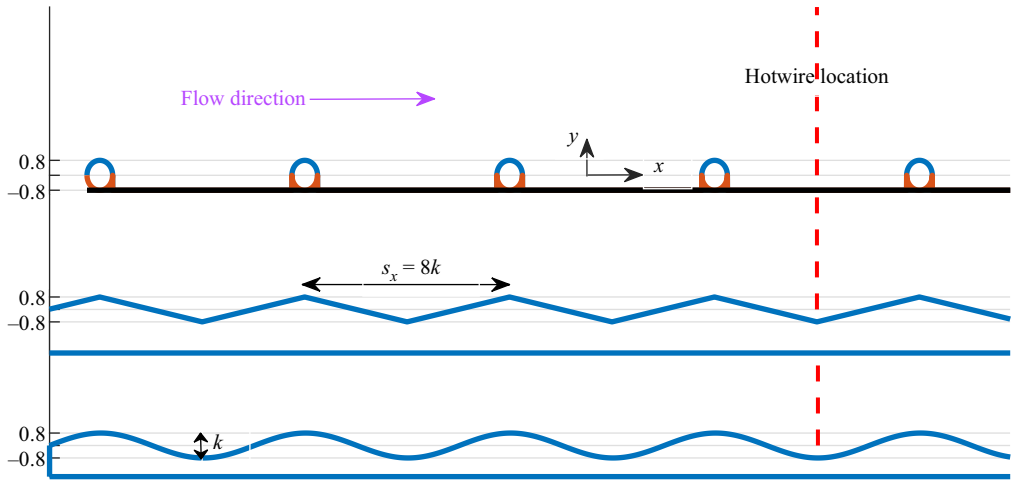


Figure 1. Schematic of different surface geometry set-ups with the same $k = 1.6$ mm and $s_x = 8k$. The red dotted line shows the measurement location. The coordinate system used in the experiments and $y = 0$ as a reference point are indicated in the schematic.

the hot-wire. A -3 dB drop off at approximately 10 kHz is recorded. Static calibration of the hot-wire is performed before and after each experiment. Calibrations are performed *in situ* against the Pitot-static tube positioned in the free-stream flow. More than 20 different velocities ranging between zero and 1.2 of the free-stream velocity of the experiment, are used for the calibration. If the pre-and post-calibrations do not collapse well, with a maximum 2 % error, the measurement is repeated. A polynomial of order six is used for fitting the voltage of the hot-wire and the measured velocity from the Pitot-static tube. Linear interpolation between pre-and post-calibrations are used to account for the hot-wire voltage drifting during the whole experiment.

A high magnification digital microscope is used to determine the offset from the wall at the first measurement point. The microscope is mounted on a 3D printed plate and placed on the rough surfaces to determine the wall offset. The probe is moved down to a distance of 100 μm over the plate before removing the plate. Then, the probe is moved down by a specific distance. This distance is equal to the thickness of the plate, plus the 100 μm offset, plus half of the roughness height $(20 + 0.1 + k/2)$ mm. Thus $y = 0$ is located at the midpoint of the roughness element height. The criterion for choosing this location is detailed in § 3. Measurements are taken at the midpoint of two consecutive roughness peaks at $x \approx 1.5$ m downstream, measured after the tripping sandpaper. A total of 48 logarithmically spaced measurement points along the wall-normal position are taken by a Mitutoyo height gauge with a linear glass encoder attached to it, with 1 μm resolution, to determine the distance travelled away from the wall accurately. Measurements are taken with a sampling rate of 35 kHz for each wall-normal location. Figure 1 shows a schematic of the different rough surface set-ups and the measurement location.

2.4. *Experiments*

Two sets of experiments are conducted. In the first set the free-stream velocity U_∞ is varied from 5 to 20 m s^{-1} over 2-D circular rods of $k = 1.6$ mm diameter and $8k$ spacing. The results are validated with data from Djenidi *et al.* (2018) with almost the same roughness, and the same Re_τ range from 1300 to 5220. The boundary layer thicknesses

https://doi.org/10.1017/jfm.2022.242 Published online by Cambridge University Press

Surface	x (m)	U_∞ (m s^{-1})	U_τ (m s^{-1})	ν/U_τ (m s^{-1})	δ (μm)	Re_τ (mm)	Re_θ	l^+	H	C_f	δ/k	k_s^+	ΔU^+
$R16-08$	1.5	5.0	0.32	47	60	1295	3080	21	1.73	0.0082	38	210	9.8
		7.0	0.45	34	60	1779	4278	30	1.72	0.0081	38	288	10.5
		10.0	0.63	24	61	2583	6189	42	1.72	0.0079	38	406	11.4
		15.0	0.93	16	63	3916	9385	62	1.72	0.0077	39	647	12.5
		19.7	1.22	12	64	5223	12435	81	1.73	0.0077	40	903	13.4
$R16-08L$	2.54	4.2	0.24	65	98	1516	3922	8	1.73	0.0065	61	220	9.6
		6.4	0.38	41	96	2340	6045	12	1.73	0.0070	62	299	10.4
		10.4	0.62	25	99	3945	9925	20	1.73	0.0072	62	450	11.5
		15.0	0.90	17	100	5766	14305	29	1.67	0.0072	63	625	12.3

Table 2. Details of the first set of rough wall experimental data. $R16-08L$ refer to Djenidi *et al.* (2018) data.

are different because of the variation of the measurement location. The details of the first set of experiments are indicated in table 2. The first set aims to validate our measurements and calculation of the friction velocity U_τ, as well as validate the fully rough Reynolds number independence and the consistency of the coefficient of friction C_f in the fully rough regime.

For the second set of experiments, measurements over different rough surfaces such as rods, triangular ribs and sinewaves, are carried out. All measurements in the second set are in the fully rough regime where $k_s^+ > 100$, with three different free-stream velocities ranging from 10 to 23 m s^{-1} for each surface. The boundary layer thickness varied from 48 to 70 mm ($23 < \delta/k < 41$). All information and details of the second set of data are presented in table 3. This set is used to investigate dominant roughness parameters that affect the turbulence statistics as well as the drag coefficient and correlate them directly to the roughness function.

3. Friction velocity

One of the challenges of turbulent boundary layer (TBL) measurements over a rough surface is the calculation of the friction velocity U_τ. Clauser (1956) introduced a method, the Clauser chart method, widely used for smooth wall TBL. The method consists of fitting measured velocity profile data to the so-called law of the wall

$$U^+ = \frac{1}{\kappa}\ln y^+ + B, \tag{3.1}$$

where κ is the von Kármán constant and B is an additive constant. Unfortunately, the method has some uncertainties, such as the values of κ, B and the lower and upper limits of the overlap region. For rough surface TBLs, the method requires two more variables, adding further uncertainties (Perry & Joubert 1963) since the law of the wall becomes

$$U^+ = \frac{1}{\kappa}\ln\frac{(y+\epsilon)U_\tau}{\nu} + B - \Delta U^+, \tag{3.2}$$

where ϵ is an origin offset.

Marusic *et al.* (2013) carried out measurements on high Reynolds number smooth wall TBLs. They found that the boundaries of the log region that best fit the velocity profiles

https://doi.org/10.1017/jfm.2022.242 Published online by Cambridge University Press

Surface	Symbol	U_∞ (m s^{-1})	U_τ (m s^{-1})	ν/U_τ (μm)	δ (mm)	Re_τ	Re_θ	l^+	H	C_f	δ/k	k_s^+	ΔU^+
Smooth	+	09.9	0.40	37	38	990	2930	15	1.35	0.0031	NA	NA	NA
	×	19.9	0.76	20	33	1640	4850	29	1.31	0.0028	NA	NA	NA
$R16-06$	■	10.0	0.62	24	59	2443	5954	42	1.69	0.0078	37	358	11.0
	■	15.0	0.92	16	60	3655	8961	61	1.69	0.0076	37	562	12.1
	■	19.5	1.19	12	61	4861	11806	79	1.70	0.0075	38	785	13.0
$R16-08$	●	10.1	0.63	24	61	2583	6189	42	1.72	0.0079	38	406	11.4
	●	15.0	0.93	16	63	3916	9385	62	1.72	0.0077	39	647	12.5
	●	19.7	1.22	12	64	5223	12435	81	1.73	0.0076	40	903	13.4
$R16-12$	♦	10.0	0.60	25	58	2353	5835	40	1.66	0.0074	37	290	10.5
	♦	14.9	0.89	16	64	3791	9273	60	1.70	0.0072	40	478	11.8
	♦	19.3	1.15	13	65	4972	12013	77	1.74	0.0071	41	708	12.9
$R16-16$	▸	10.1	0.60	25	60	2412	5866	40	1.61	0.0071	38	240	10.3
	▸	15.0	0.89	17	62	3689	9379	59	1.63	0.0070	39	450	11.5
	▸	19.8	1.17	13	62	4804	12427	78	1.65	0.0070	38	679	12.3
$R16-24$	◂	10.0	0.58	26	55	2112	5412	38	1.60	0.0066	34	181	09.3
	◂	15.0	0.85	18	57	3256	8231	57	1.60	0.0065	36	270	10.5
	◂	19.4	1.10	14	54	3999	10406	74	1.61	0.0065	34	379	11.1
$R24-06$	■	10.0	0.63	24	69	2873	6804	42	1.72	0.0079	29	445	11.7
	■	14.9	0.93	16	70	4330	10380	62	1.70	0.0077	29	740	12.9
	■	20.0	1.24	12	69	5702	13696	83	1.70	0.0076	29	1039	13.7
$R24-08$	●	09.9	0.63	24	65	2754	6524	42	1.78	0.0082	27	510	11.9
	●	14.9	0.92	16	66	4049	9967	61	1.76	0.0077	27	678	12.7
	●	19.7	1.22	12	66	5321	12702	81	1.77	0.0077	27	1026	13.7
$R24-12$	♦	09.6	0.60	25	61	2435	5939	40	1.74	0.0078	25	373	11.0
	♦	14.7	0.89	17	62	3699	9044	60	1.73	0.0074	26	548	12.0
	♦	19.3	1.15	13	63	4858	11944	77	1.73	0.0071	26	697	12.7
$R24-16$	▸	10.0	0.60	25	65	2592	6254	40	1.66	0.0072	27	286	10.7
	▸	14.9	0.89	17	66	3897	9592	59	1.65	0.0071	27	482	11.9
	▸	20.1	1.17	13	65	5070	12434	78	1.64	0.0068	27	547	12.4
$R24-24$	◂	09.9	0.57	26	55	2090	5371	38	1.57	0.0066	23	168	09.2
	◂	15.0	0.84	18	60	3361	8554	56	1.57	0.0063	25	255	10.3
	◂	19.9	1.12	13	58	4307	11087	75	1.57	0.0063	24	351	11.1
$T16-08$	▲	12.0	0.67	22	53	2374	6102	45	1.60	0.0062	33	164	09.1
	▲	14.9	0.82	18	54	2977	7777	55	1.59	0.0061	34	199	09.6
	▲	19.6	1.06	14	53	3738	9681	71	1.59	0.0059	33	234	10.1
$S16-08$	▾	14.9	0.81	19	48	2596	6652	54	1.59	0.0058	30	139	08.8
	▾	19.9	1.06	14	50	3542	9182	70	1.59	0.0057	31	181	09.6
	▾	22.7	1.20	12	52	4141	10515	80	1.61	0.0057	32	218	10.2
$S24-08$	▾	10.1	0.54	28	59	2139	5511	25	1.52	0.0057	25	95	08.0
	▾	15.0	0.80	19	63	3347	8495	37	1.52	0.0057	26	159	09.4
	▾	20.0	1.07	14	65	4683	11722	50	1.51	0.0057	27	237	10.8

Table 3. Details of the second set of rough wall experimental data.

https://doi.org/10.1017/jfm.2022.242 Published online by Cambridge University Press

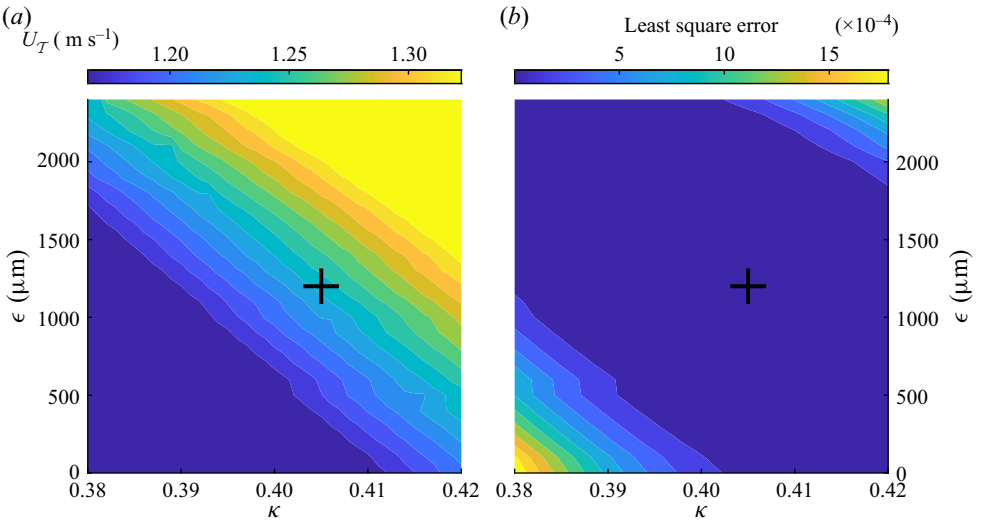


Figure 2. Friction velocity and least square error of TBL measurement over the $R24-06$ surface at $Re_\tau = 5700$. (a) Contours of U_τ calculated from the modified Clauser chart. (b) Contours of least squares error from fitting data to the modified Clauser chart. The plus mark (+) refers to $\kappa = 0.405$ and $\epsilon = k/2 = 1200$ μm.

are $y^+ > 3\sqrt{Re_\tau}$ and $y/\delta = 0.15$, which will be adapted in the present study as they best fit the log region of the velocity profiles over rough surfaces as well. Recently, Djenidi, Talluru & Antonia (2019) proposed a method for estimating U_τ for both smooth and rough wall TBLs. The method assumes an outer layer similarity between the smooth and rough flow and uses the velocity defect distribution, which is shown to exhibit a universal form for these two TBLs. A practical advantage of this latter method is that it involves empirical constants, thus eliminating the uncertainties of the modified Clauser chart method.

In the present work both the modified Clauser chart (Perry & Li 1990) and the velocity defect chart (Djenidi *et al.* 2019) methods will be used. Regarding the modified Clauser chart method, we performed a detailed study of the effect of κ and ϵ on the estimate of U_τ, in an attempt to understand how these parameters affect the results. Estimates based on both methods are compared. Figure 2(a) shows the values U_τ, based on the modified Clauser chart, for different values of ϵ and κ over the $R24-06$ surface at $U_\infty = 20$ m s^{-1}; ϵ varies from 0 to k while κ ranges from 0.38 to 0.42. The least squares error of the fitting equation in the log region is shown in figure 2(b). Results for different free-stream velocities and different surface roughnesses follow the same pattern of contours and are not shown here. These contours also show an infinite number of solutions that can be fitted with the same least squares error, illustrating the strong reliance on ϵ and κ of the modified Clauser chart method, and thus somehow its weakness. Figure 2(a) indicates that the maximum deviation for U_τ when using the modified Clauser chart is approximately 10 %. Figure 2(b) shows that $\kappa \approx 0.4$ gives the smallest error, regardless of the value of ϵ. Also, using $k/2 < \epsilon < 3k/4$ yields the same minimum error from fitting the mean velocity profile by the modified Clauser method regardless of the value of κ. The roughness function ΔU^+ is determined by averaging the vertical shift between the log region ($y^+ > 3\sqrt{Re_\tau}$ to $y/\delta = 0.15$) of the rough wall and smooth wall wall-unit normalised velocity profiles.

Since the main goal of the present study is to compare various roughness geometries and the focus of the results is on the outer layer similarity, we fix $\epsilon = k/2$ for all rough

https://doi.org/10.1017/jfm.2022.242 Published online by Cambridge University Press

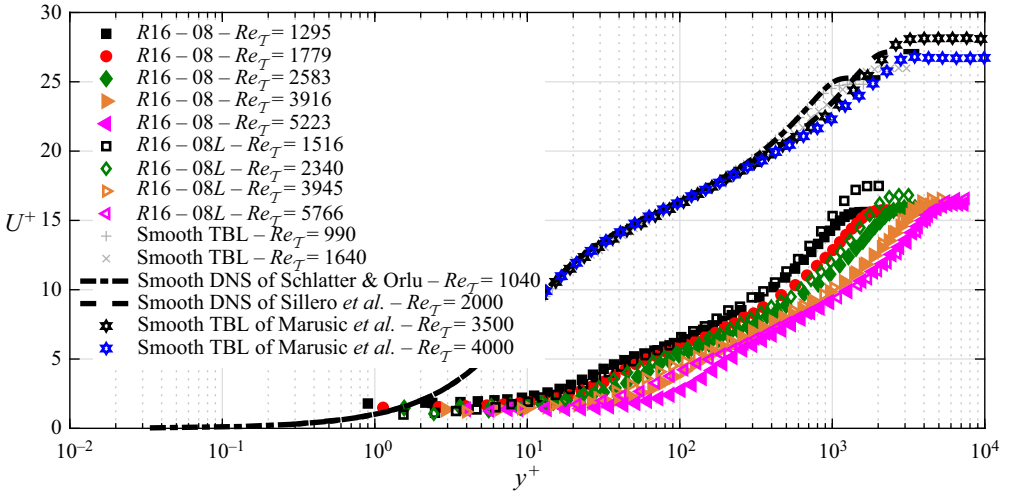


Figure 3. The streamwise mean velocity profiles over the $R16-08$ surface at different free-stream velocities normalised by the friction velocity U_τ. The unfilled symbols represent data from Djenidi *et al.* (2018) at the closest Re_τ. Our smooth wall TBL measurements are plotted in grey symbols and are detailed in table 3. The dot-dashed line shows the smooth DNS data from Schlatter & Örlü (2010) at $Re_\tau = 1040$. The dashed line shows the smooth DNS data from Sillero *et al.* (2014) at $Re_\tau = 2000$. The black and blue hexagram symbols are smooth TBL data from Marusic *et al.* (2015) at $Re_\tau = 3500$ and 4000, respectively. The wall-normal position y is normalised by the inner length scale ν/U_τ.

walls under investigation with $\kappa \approx 0.405$ and $B = 5$. Fixing these values, we found that U_τ obtained from the modified Clauser chart method matches that obtained from the velocity defect chart with an error of less than 3 % for all Reynolds numbers considered. The value of U_τ obtained from the velocity defect chart is used in the presented results for all rough wall flows, since the values obtained from both methods show good agreement.

4. Results

4.1. *Validation*

Streamwise mean velocity profiles of the TBL over the $R16-08$ surface, normalised by inner scaling parameters at different Re_τ, are plotted with filled symbols in figure 3. For comparison with our measurements, the data of Djenidi *et al.* (2018) at comparable Re_τ are represented with unfilled symbols. Also, our smooth wall data measurements are compared with the smooth TBL direct numerical simulation (DNS) data of Schlatter & Örlü (2010) and Sillero, Jiménez & Moser (2014) for $Re_\tau = 1040$ and $Re_\tau = 2000$, respectively. Two sets of smooth wall TBL experimental data (Marusic *et al.* 2015) are also reported on the figure for comparison. As expected, all smooth wall data collapse very well in the buffer and log regions. The friction velocity for smooth wall measurements is calculated by the Clauser method with $\kappa = 0.405$ and $B = 5$.

Using 2-D cylindrical rods for roughening a surface leads to a fully rough regime at a relatively low Re_τ. All rough data in figure 3 are in a fully rough regime, as indicated in table 2. Increasing Re_τ, or equivalently U_∞, once the fully rough regime is achieved causes a rightwards shift towards larger y^+, while $U^+ = U/U_\tau$ (or $C_f \sim \sqrt{U_\tau/U}$) remains constant. The present data are in good agreement with the data of Djenidi *et al.* (2018), especially at Re_τ higher than 4000. The rightwards shift towards

https://doi.org/10.1017/jfm.2022.242 Published online by Cambridge University Press

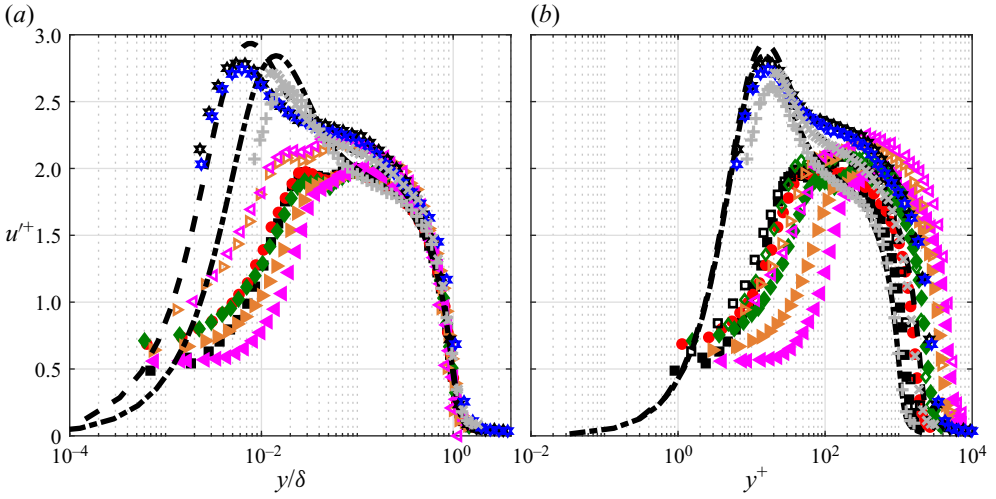


Figure 4. Profiles of u' over the $R16-08$ surface at different free-stream velocities normalised by the friction velocity U_τ. The symbols are the same as indicated in figure 3. (*a*) The wall-normal position y is normalised by the outer length scale δ. (*b*) The wall-normal position y is normalised by the inner length scale ν/U_τ.

larger y^+ while maintaining the same C_f suggests that the inner length scale ν/U_τ is not an adequate scaling length for rough wall mean streamwise velocity profiles.

Profiles of streamwise root-mean-square (r.m.s.) velocity fluctuating u'^+ for the $R16-08$ surface are reported in figures 4(*a*) and 4(*b*) as functions of y/δ and $y/U_\tau/\nu$, respectively. Figure 4(*a*) shows an excellent collapse in the outer layer $y/\delta > 0.6$, regardless of the Reynolds number or the roughness of the surface. The present rough and smooth wall data exhibit lower magnitudes than those of Djenidi *et al.* (2018) and Marusic *et al.* (2015) in the near-wall region. This is believed to be due to larger values of our l^+, which may attenuate the actual values of u'^+. Nevertheless, this has a negligible effect on the scope of the work as our focus is on comparing different kinds of roughnesses in terms of their effects on the mean velocity profiles. Chin *et al.* (2009) investigated spatial resolution issues in hot-wire measurements of wall-bounded turbulent flows. They applied different spanwise filter lengths to channel flow DNS data streamwise velocity components to simulate different spatial resolutions of single hot-wire probes. They found that the most severe attenuation occurs in the near-wall region due to the dominance of the small turbulence scales in this region. These attenuations are less severe in the outer region and are practically negligible for $y/\delta > 0.6$.

Figure 4(*b*) shows a noticeable systematic shift of the u'^+ profiles when plotted as a function of y^+. The rightward shift is similar to that observed in U^+ as Re_τ increases, further confirming that the inner length scale ν/U_τ is not an appropriate scaling length. For the rough wall data, one can observe a local inner peak at low Reynolds which tends to vanish as the Reynolds number increases. This behaviour is consistent with that observed in Schultz & Flack (2007), Krogstad & Efros (2012), Squire *et al.* (2016) and Djenidi *et al.* (2018), further indicating that the possible attenuation associated with the relatively large values of l^+ does not critically affect the data, at least qualitatively in the inner region, giving us confidence in our measurements.

https://doi.org/10.1017/jfm.2022.242 Published online by Cambridge University Press

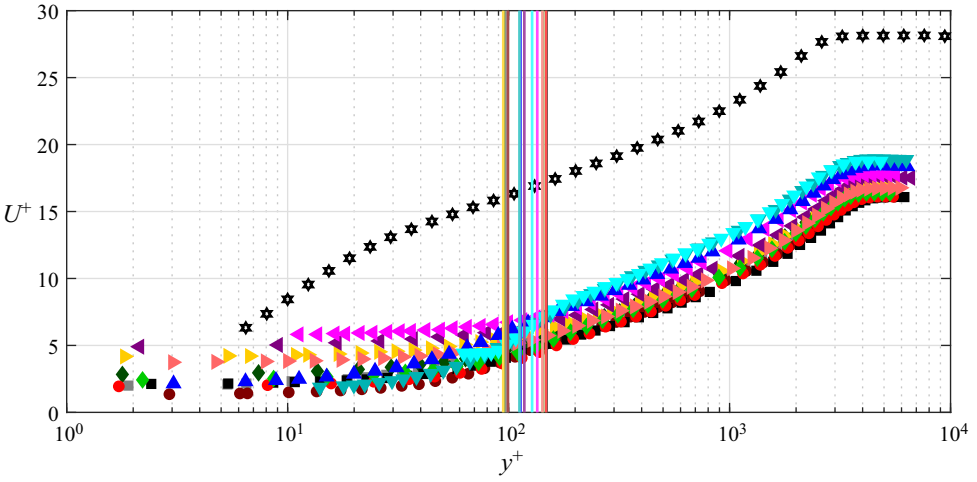


Figure 5. Streamwise mean velocity profiles over different rough surfaces at matched Reynolds number $3300 < Re_\tau < 4300$ where each surface is normalised by the friction velocity U_τ. The symbols of our measurements are detailed in table 3. The black hexagram symbols are smooth TBL data from Marusic *et al.* (2015) at $Re_\tau = 3500$. The wall-normal position y is normalised by the inner length scale ν/U_τ. The vertical lines indicate the roughness heights in terms of viscous length scale units k^+.

4.2. *Second set of experiments*

4.2.1. *Mean velocity profile*

Figure 5 shows the distributions U^+ vs y^+ for all the different rough surfaces used in this study; the vertical lines correspond to $y = k$ and their colours match those of the profiles they are associated with. For each rough wall, only one velocity distribution corresponding to a fully rough regime is reported; Re_τ ranges from 3300 to 4300. Also, the smooth wall velocity distribution data of Marusic *et al.* (2015) at $Re_\tau = 3500$ are shown in the figure as reference.

As we mentioned earlier, in a fully rough regime and at high Reynolds numbers, increasing the Reynolds number simply shifts the mean velocity profile to the right, to larger y^+, while C_f remains constant. Roughnesses with the same spacing ratio s_x/k are represented by the same symbol, while the colours indicate different roughness heights, as indicated in table 3. If we consider the rod and sinewave roughnesses and consult table 1, we note that keeping s_x constant while changing k does not change k_{sk}, k_{ku}, ES and λ_f. Thus, the excellent collapse we observe between the distribution s_x for the rod and sinewave rough wall suggests that, in the fully rough regime, changing k or δ/k does not affect the mean streamwise velocity profile if δ/k is large enough ($\delta/k > 23$ in the present case). Changing of the spacing ratio between rods from 6 to 24 while maintaining the same roughness height causes a downward shift as a result of an increase of C_f. Decreasing the s_x/k ratio, which results in an increase of the effective slope ES and a decrease of the skewness k_{sk} for the same geometry, leads to a larger C_f with a resulting downward shift. More details about the effect of roughness parameters on the coefficient of friction will be discussed later, in § 4.2.4.

The velocity profiles for the rods with spacing ratios of 6 and 8 collapse relatively well, indicating that the boundary layer is only marginally affected by the small change of s_x, which is illustrated by the fact that C_f values for both spacing ratios are practically the

https://doi.org/10.1017/jfm.2022.242 Published online by Cambridge University Press

same (see table 3). This is consistent with DNS data of Leonardi *et al.* (2003) which show that the drag in a rod roughened turbulent channel flow is practically unchanged for $6 \leq s_x/k \leq 8$. Similar results are also observed in the data for a TBL over a rod roughened wall in Furuya, Miyata & Fujita (1976). Although sinewave and triangular rib geometries have comparable sizes to the rods, ($k = 1.6$ or 2.4 mm and $s_x = 8k$), they exhibit the lowest C_f and ΔU^+ (see table 3), resulting in a reduced downward shift for the corresponding velocity profiles in comparison with those for the rods.

The above observation applies to the region $y > k$. Since the distributions are only local ones (taken midway between two roughness elements), one expects to observe differences in the region $y < k$. These differences, however, disappear quite rapidly as y increases above k. For example, all the profiles exhibit almost the same shape when $y^+ \geq 200$. It is interesting to note that all the present rough surfaces have a similar wall-unit roughness height $100 < k^+ < 150$, while C_f varies from 0.0057 to 0.0077. This would confirm that roughness height alone is not a suitable roughness parameter to characterise the roughness function or the roughness geometry. This appears to be confirmed by the data of Krogstad & Efros (2012) and the data of Djenidi *et al.* (2018). Other parameters, such as ES and k_{sk}, may be more appropriate. This will be discussed in § 4.2.4 below.

Figure 6 shows the mean streamwise velocity profiles normalised by different outer length scales for all the different rough surfaces used in this study. While for a given roughness geometry the corresponding profiles collapse regardless of the length scale used, the situation is different when we consider all roughness geometries together. Indeed, a lack of a general collapse is observed when the length scales k and δ are used, as shown in figures 6(*a*) and 6(*b*), respectively. This clearly indicates that the roughness height alone is not sufficient parameter to characterise the surface roughness. A similar remark has been made by Squire *et al.* (2016) and Djenidi *et al.* (2018) who argued that an outer length scale cannot be used to collapse velocity profiles normalised by the inner velocity scale when considering different kinds of roughnesses. However, when the equivalent sand grain roughness k_s is used the profiles appear to collapse better, as seen in figure 6(*c*). This suggests that, even though k_s has no real physical meaning, it is nevertheless commonly used to characterise roughness. In that aspect, it is, from an engineering point of view, a very useful roughness length scale.. Unfortunately, its lack of physical meaning makes it impossible to measure it directly from the topology of the surface. Nevertheless, there are attempts to correlate this parameter with the actual roughness parameters (Schultz & Flack 2009; Flack *et al.* 2020). Unfortunately, none of these attempts provides a universal k_s that can be used for all kinds of roughness geometries. This, however, does not preclude the possibility of proposing a k_s that can be valid for a given family of a roughness geometries. In the next section we attempt to develop an expression for k_s for 2-D roughness.

4.2.2. *Roughness function*

Roughness has a wide range of shapes, types and textures that makes it almost impossible to characterise it by a single physical roughness parameter. Firstly, we need to define, if possible, the major roughness parameters that mostly affect the drag. Then, develop an equation for the equivalent sand grain roughness k_s that combines these parameters. The most common roughness parameter used to characterise the roughness is its height. There are various heights that can be measured from the roughness topography such as the average roughness height k_a, the root-mean-square roughness height k_{rms}, the maximum peak to valley roughness height k and the average of the highest 5 roughness peaks to

https://doi.org/10.1017/jfm.2022.242 Published online by Cambridge University Press

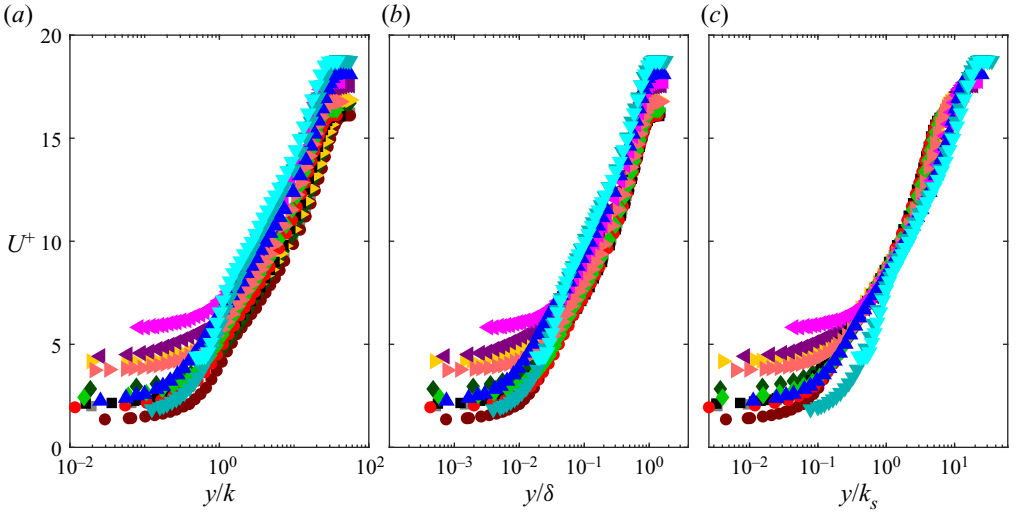


Figure 6. The streamwise mean velocity profiles over different rough surfaces at matched Reynolds number $3300 < Re_\tau < 4300$ where each surface is normalised by the friction velocity U_τ. The wall-normal position y is normalised by different outer length scales. The symbols of the different rough surfaces are detailed in table 3. (*a*) The wall-normal position y is normalised by the outer roughness length scale k. (*b*) The wall-normal position y is normalised by the outer length scale δ. (*c*) The wall-normal position y is normalised by the outer roughness length scale k_s.

the maximum lowest valleys k_z (ASME 2009). However, none of these roughness height parameters are alone capable of describing the roughness completely.

Figure 7 shows ΔU^+ as a function of maximum peak-to-valley roughness height, k, for all the different surfaces used in this study. Each rough surface has different ΔU^+ in the fully rough regime, and there is no corresponding map function between the roughness height and the roughness function. All the surfaces used in this study only have two maximum peak to valley heights, even though the wall drag changes from one surface to another. Hence, another family of roughness parameters must be employed.

The frontal solidity λ_f is defined as the ratio of the total projected frontal area to the total plan area. This parameter indicates how big the area exposed to the flow is, which can be directly related to the pressure drag (MacDonald *et al.* 2016). Napoli *et al.* (2008) introduced the effective slope ES, defined as the mean absolute gradient of a roughness surface $ES = 2\lambda_f$. The advantage of using ES over λ_f is that the gradient can be calculated for any surface, even for random roughnesses, which makes it more general and robust in characterising the roughness.

Figure 8 shows ΔU^+ as a function of ES. It can be seen that, for the rods, ΔU^+ increases with ES. Note that the roughness function for triangular rib and sinewave surfaces is much lower than rods that have the same ES. This may be due to the fact that $k_{sk} = 0$ for the former roughnesses. The data of Napoli *et al.* (2008), who carried out a large eddy simulation of a rough wall turbulence channel flow, are reported in figure 8. Their roughness consisted of corrugated walls covering a wide range of ES. We observe that our sinewave roughness functions match very well with their data. This validates the argument concerning the importance of the effective slope in determining the roughness function as well as in validating our measurements. The message of figure 8 is that, for a fixed ES, highly skewed surfaces, such as rods, have higher roughness functions than

https://doi.org/10.1017/jfm.2022.242 Published online by Cambridge University Press

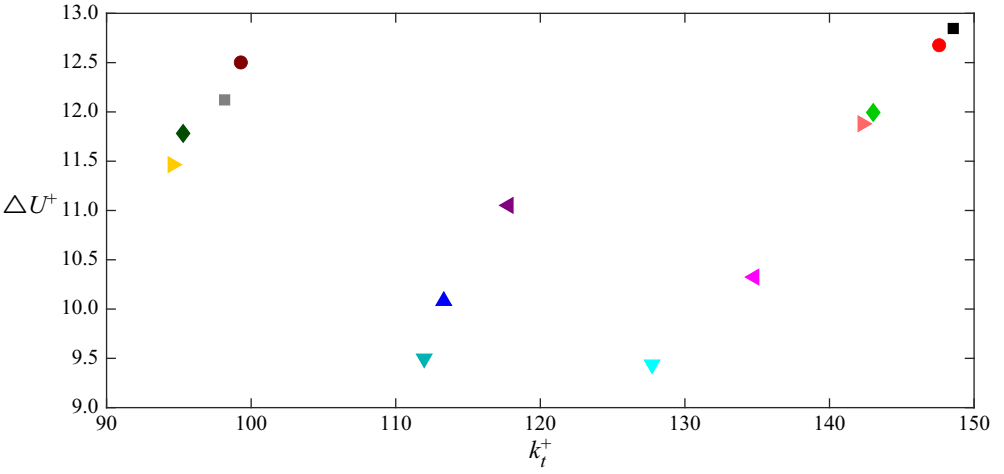


Figure 7. Roughness function ΔU^+ as a function of maximum peak-to-valley roughness height, k, normalised by the inner length scale ν/U_τ. The filled symbols are the different surfaces roughness symbols indicated in table 3.

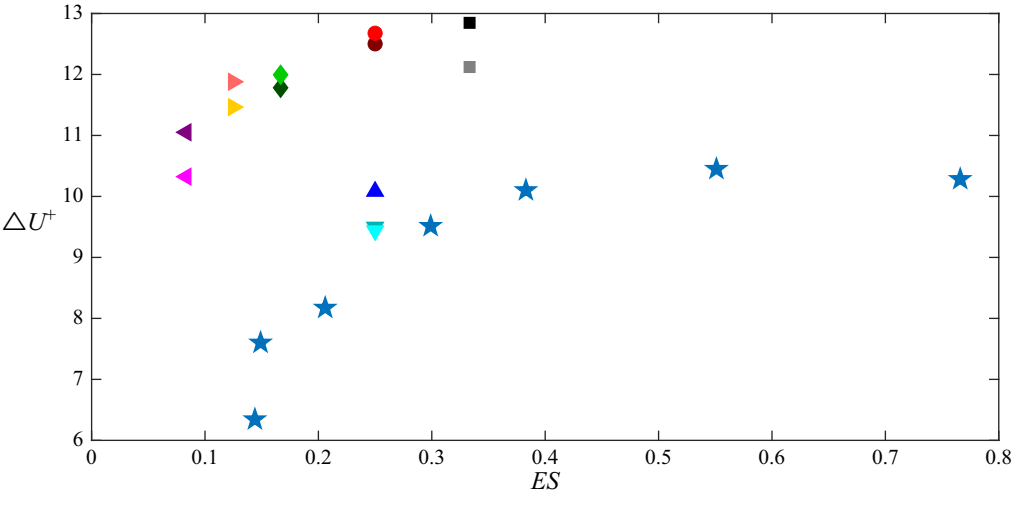


Figure 8. Roughness function ΔU^+ as a function of effective slope, ES. The filled symbols are the different surfaces roughness symbols indicated in table 3. The blue pentagram symbols are channel flow data over various irregularly distributed sinusoidal roughness from Napoli *et al.* (2008).

corrugated-like surfaces. Further information one can infer from the figure is that it is challenging to describe a surface with only one roughness parameter. This reinforces the idea that a combination of two or more roughness parameters is likely to be needed to adequately characterise roughnesses. Although roughness height and slope reveal most of the roughness characteristics, they are not sufficient to completely describe the roughness.

Figure 9 shows the streamwise mean velocity profiles over $R16-08$, $S16-08$ and $T16-08$ surfaces. These three surfaces have the same roughness height, k, and the same effective slope, ES, but different geometries. The roughness functions, ΔU^+, for $S16-08$ and $T16-08$ are almost the same, however, they have lower ΔU^+ than $R16-08$.

https://doi.org/10.1017/jfm.2022.242 Published online by Cambridge University Press

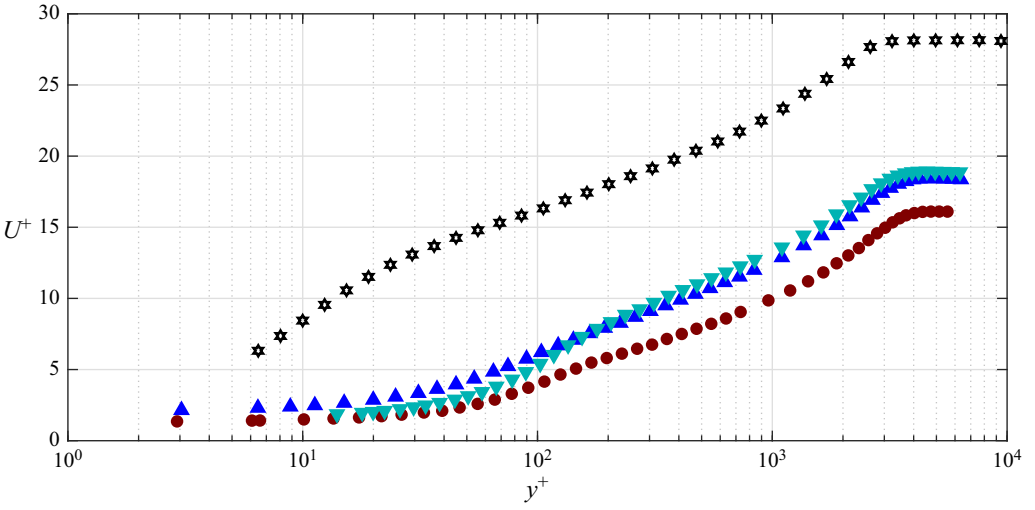


Figure 9. The streamwise mean velocity profiles over three different roughnesses with the same height, k, and effective slope, ES, but different geometries normalised by the friction velocity U_τ. Cases $R16-08$, $S16-08$ and $T16-08$ are compared with the smooth TBL data from Marusic *et al.* (2015). The symbols of our different surfaces are indicated in table 3.

If we consider these roughnesses and consult table 1 we note that the skewness, k_{sk}, of the sinewave and the triangular ribs is the same, but different from the rods. Hence, a third group of roughness parameters should be introduced to adequately describe the roughness.

The plan solidity, λ_p, is defined as the ratio of the total projected plan area to the total plan area. This parameter measures how dense the roughness is (Placidi & Ganapathisubramani 2015). As mentioned above, ES is more usable than λ_f and can be used even for random roughness, the skewness of the roughness is more usable than the plan solidity and can be used for regular and irregular roughnesses. The skewness measures the symmetry of a profile about the mean line. It indicates a morphology of the surface texture; $k_{sk} > 0$ corresponds to high peaks, while $k_{sk} < 0$ corresponds to pitted surfaces.

Figure 10 shows ΔU^+ as a function of k_{sk} in the fully rough regime. It can be noticed that, for the rods only, the roughness function decreases with increasing roughness skewness. The roughness functions for triangular rib and sinewave surfaces have lower values than rods, as they have zero roughness skewness value.

Attempts to correlate the k_s with roughness parameters like k_{sk}, and k_{rms} have been carried out (see Flack *et al.* 2016). Others proposed to relate ΔU^+ to ES instead of k_s (Napoli *et al.* 2008). However, a review of these different proposals shows that they apply to particular roughness geometries. This raises an interesting practical issue concerning whether these roughness parameters can be related to k_s, which controls the roughness function ΔU^+ as follows (Nikuradse 1933):

$$\Delta U^+ = \frac{1}{\kappa}\log(k_s^+) + B - 8.5. \tag{4.1}$$

In the following analysis we use $\kappa = 0.405$ and $B = 5$ and only data for which $\Delta U^+ > 8.5$ are used to compute k_s^+. It would seem that a combination of the three roughness parameters (k, ES and k_{sk} would provide a better correlation function for k_s.

https://doi.org/10.1017/jfm.2022.242 Published online by Cambridge University Press

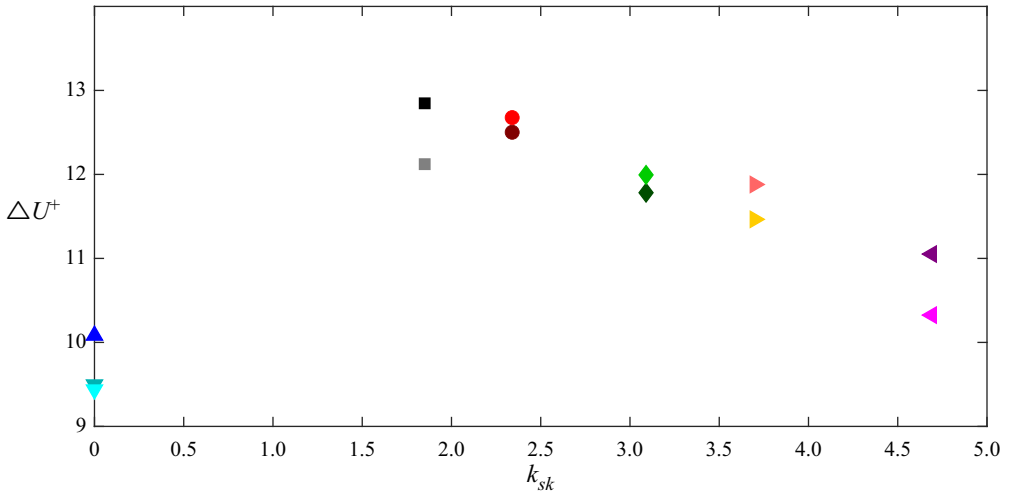


Figure 10. Roughness function ΔU^+ as a function of roughness skewness, k_{sk}. The filled symbols are the different surfaces roughness symbols indicated in table 3.

Figure 11 suggests that the expression (4.2) provides a suitable empirical relation for k_s for 2-D roughness. It is thus of interest to assess how this relation compares with previous experimental and numerical results for k_s. This comparison is reported in figure 12, which shows the present predicted values of k_s with those of Krogstad & Efros (2012), Djenidi *et al.* (2018) and Leonardi *et al.* (2003). In this figure, a perfect agreement between the present predictions and measurement is represented by a straight line. While there is some scatter in the data, the figure shows a clear trend: the data align relatively well with the straight line, providing support for (4.2)

$$k_s = a + b \times k + c \times \frac{2k}{ES} + d \times ES \times k_{sk}, \tag{4.2}$$

where $a = 0.001$, $b = 1.865$, $c = -0.103$, $d = 0.013$, with $R^2 = 0.93$. here, R^2 is a statistical measure of how close the data are to the fitted regression line. It can be noticed that $2k/ES = s_x$ for uniform distributed roughness. It can be observed that, when $k_{sk} = 0$, as for sinewaves or triangular ribs, k_s will depend only on the roughness height k and the spacing between two consecutive roughness peaks s_x for distributed 2-D roughness or the effective slope for random roughness. However, for highly positive skewed roughness like 2-D cylindrical rods, both k_{sk} and ES affect k_s and are accounted for by the last term of (4.2). All data in the fully rough regime are on Nikuradse's asymptote line. These data support the proposal that k_s correlates very well with the drag coefficient ΔU^+ in the fully rough regime. Remarkably, a very good agreement is observed between ΔU^+ obtained using the measured and predicted values of k_s^+, indicating that (4.2) provides a suitable equation for predicting k_s for a family of 2-D rough surfaces, i.e. 2-D cylindrical rod roughnesses and 2-D sinewaves or triangular ribs. This linear equation is developed for uniform 2-D roughnesses with ES varying from 0.08 to 0.33 and positive skewness roughness $0 \leq k_{Sk} \leq 4.7$.

Since this empirical relation (4.2) has been developed for 2-D roughness, it was observed that it was not valid for 3-D roughness. Instead, a new empirical relation was developed for the 3-D roughness. Using the data of Flack *et al.* (2020), Barros, Schultz & Flack (2018), Busse, Thakkar & Sandham (2017), Forooghi *et al.* (2017) and Squire *et al.* (2016) and the

https://doi.org/10.1017/jfm.2022.242 Published online by Cambridge University Press

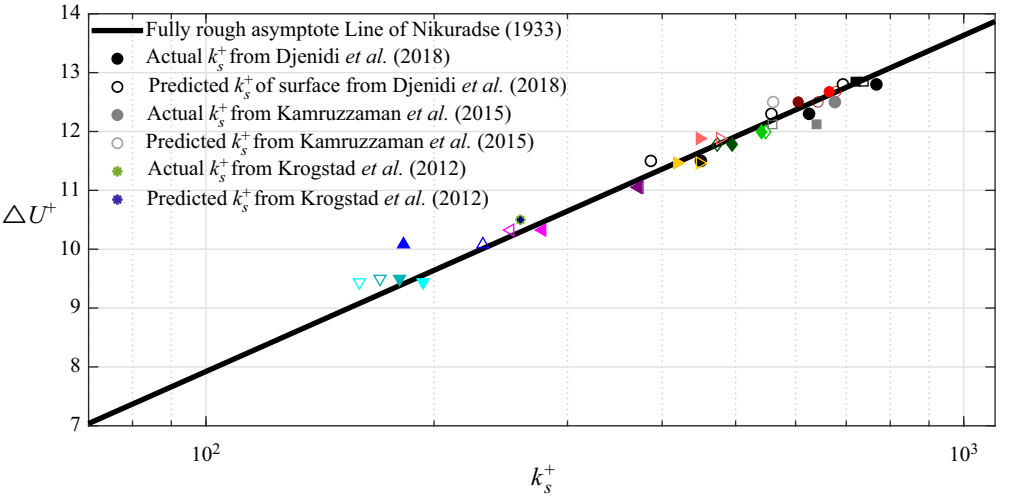


Figure 11. The roughness function for 2-D roughness as a function of equivalent sand grain roughness height k_s, normalised by the inner length scale ν/U_τ. The filled symbols are the different surface roughness symbols indicated in table 3. The unfilled symbols are the predicted k_s^+ values from (4.2) for the same rough surface. The black solid line is the fully rough asymptote of Nikuradse (1933). The values of k_s of Krogstad & Antonia (1999), Kamruzzaman *et al.* (2015) and Djenidi *et al.* (2018) are reported in the figure for comparison and validation.

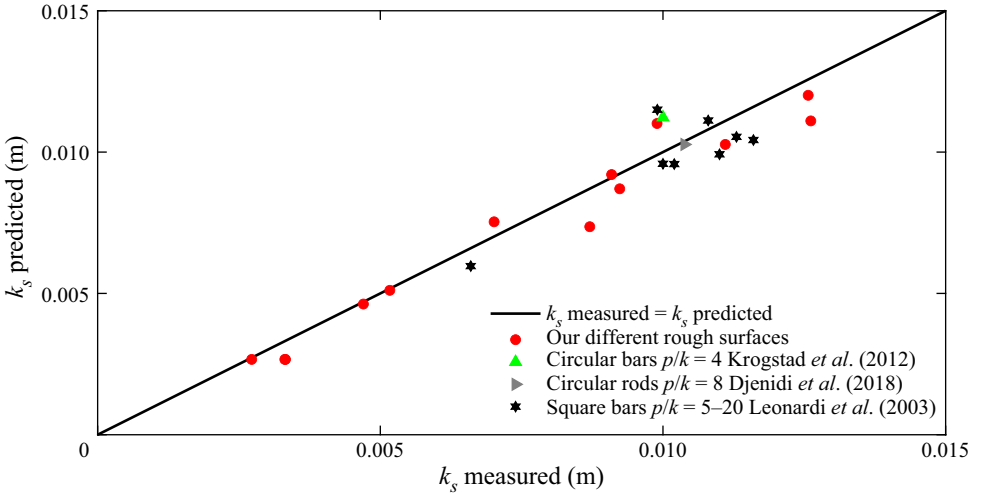


Figure 12. Comparison between actual k_s measured from mean velocity profiles and the calculated k_s from (4.2) for our surfaces along with previous experimental and numerical results for 2-D roughness only.

same physical roughness parameters used for 2-D roughness (k, k_{sk} and ES), we obtained the following empirical relation:

$$k_s = a + b \times k + c \times k_{sk} + d \times \frac{2k}{ES} + e \times ES \times k_{sk}, \tag{4.3}$$

where $a = -0.000025$, $b = 1.654$, $c = 0.004$, $d = -0.2$, $e = -0.0009$ with $R^2 = 0.79$. Notice the addition of a fifth term. Figure 13 compares the prediction of k_s using (4.3)

https://doi.org/10.1017/jfm.2022.242 Published online by Cambridge University Press

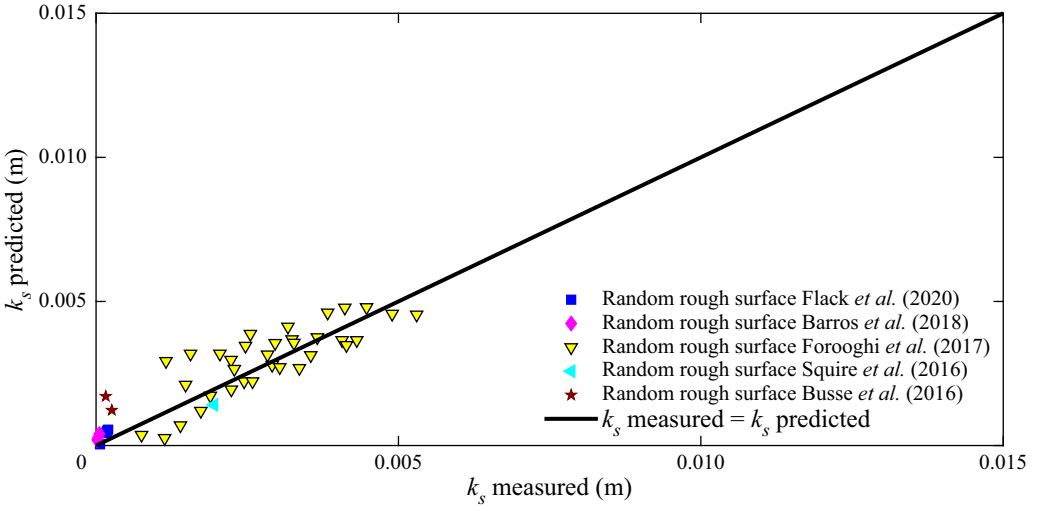


Figure 13. Comparison between actual k_s from the literature and the calculated k_s from (4.3) for 3-D roughness only.

with the values of k_s for the same data used to develop (4.3). While the data tend to exhibit an alignment with the straight line, there is a stronger scatter than in figure 12, as quantified by a lower value of R^2. The fact that two separate relations are required for the 2-D and 3-D roughnesses suggests that it is unlikely that one can develop a truly universal relation for k_s. We nevertheless attempted to obtain an empirical relation for both the 2-D and 3-D data. The result was the following relation:

$$k_s = a + b \times k + c \times \frac{2k}{ES} + d \times \frac{2k}{ES}^2 + e \times \mathrm{e}^{f \times ES \times k_{sk}}, \tag{4.4}$$

where $a = -0.002$, $b = 0.926$, $c = 0.283$, $d = 4.933$, $e = 0.001$, $f = 3.66$, with $R^2 = 0.87$.

Notice that, conversely to the two previous relations, (4.4) is nonlinear; it was not possible to obtain a linear function that yields a reasonable fit to the data. Figure 14 shows the comparison between the predicted values of k_s with the measured ones. The data exhibit a large scatter around the straight line, even though the data show a tendency to align with that line, particularly the 2-D rough wall data.

It is important to stress that, like k_s itself, empirical relations like (4.2), (4.3) and (4.4) bear no physical meaning. However, their relevance and usefulness, from an engineering viewpoint, lie in the fact that they relate physical quantities for characterising the roughness geometry. Thus, the ability to predict k_s, which can be related to the drag, using simply the roughness parameters has an obvious practical interest.

More experiments for various kinds of roughnesses (2-D roughness such as grooves instead of rods to include negative skewness roughness as well as 3-D sinusoidal and random roughnesses) are needed to either validate and/or improve the previous expressions and to determine whether a universal formula for k_s can be developed for all kinds of roughness geometries.

https://doi.org/10.1017/jfm.2022.242 Published online by Cambridge University Press

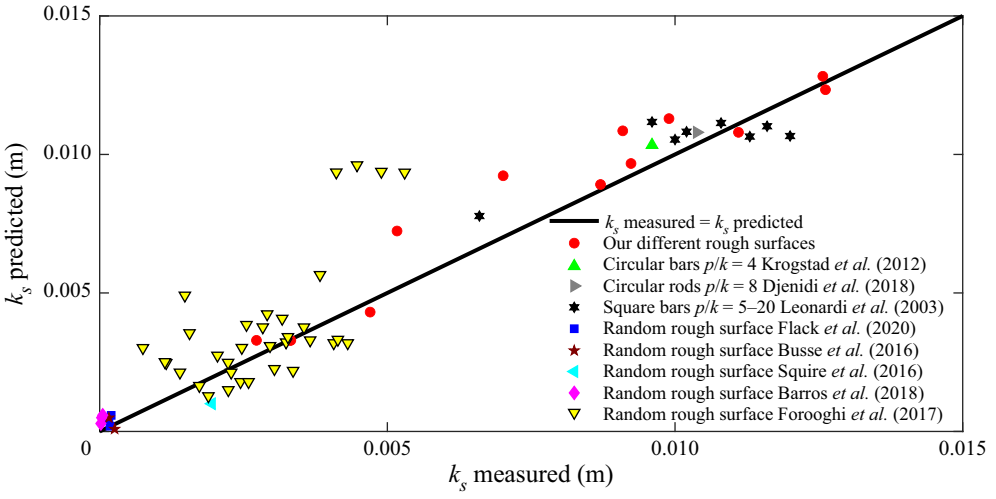


Figure 14. Comparison between actual k_s and the calculated k_s from (4.4) for 2-D and 3-D roughnesses.

5. Conclusions

Measurements are performed in a ZPG rough wall TBL to investigate the effect of different roughness parameters. Single hot-wire probes are used to measure the streamwise velocity at various Reynolds numbers and for 2-D roughness geometries. Circular rods with two different heights, $k = 1.6$ and 2.4 mm, and five different streamwise spacing ratios ranging from 6 to 24, 3D printed triangular ribs with heights of $k = 1.6$ mm and a spacing of $8k$ and CNC machined sinewave surfaces with two different heights, $k = 1.6$ and 2.4 mm, and a spacing ratio of 8 were investigated. These surface roughnesses covered a wide range of δ/k ranging from 23 to 41 in the fully rough regime.

The roughness causes a downward shift of the wall-unit normalised mean velocity profile, known as the roughness function. The maximum downward shift is reached when the spacing ratio between two roughness elements is approximately 8. Changing the roughness height, while maintaining the same spacing ratio, does not affect the drag coefficient in the fully rough regime. Varying δ/k does not affect the mean streamwise velocity profile, if δ/k is large enough; $\delta/k > 23$ in this study. This reveals that roughness height is not an appropriate parameter to characterise the roughness.

An excellent collapse of the log region in the mean velocity profiles is observed when the equivalent roughness length scale k_s is used as a length scale to normalise the mean velocity profiles. Further, while k_s is not an actual physical roughness parameter that can be measured directly from the topology of the surface, a new expression for k_s involving the physical roughness parameters k, ES and k_{sk} is proposed. It is shown that this new empirical relation provides a promising practical means to calculate the roughness function directly from the roughness topography in 2-D uniformly distributed rough surfaces. The relation shows that k, ES and k_{sk} are major surface roughness parameters affecting the turbulence statistics and drag coefficient.

Our results indicate that such general scaling cannot exist because of the complexity of the roughness geometries which involve too the many parameters. Further, the results suggest it is likely each family of roughnesses (for example 2-D roughness, 3-D roughness) would have its own scaling.

https://doi.org/10.1017/jfm.2022.242 Published online by Cambridge University Press

It should be noted that this new relation for k_s is limited to 2-D uniformly distributed roughness in a fully rough regime and more experiments on 2-D and 3-D rough surfaces, as well as random roughness, are needed to assess the importance of k, ES and k_{sk} in the turbulence statistics and drag coefficient. Such studies will help develop a more generalised relation for k_s, if such a generalisation can be made.

Funding. The authors acknowledge the financial support of the Australian Research Council.

Declaration of interests. The authors report no conflict of interest.

Author ORCIDs.
Misarah Abdelaziz https://orcid.org/0000-0003-2417-1755;
L. Djenidi https://orcid.org/0000-0001-8614-3595;
Rey Chin https://orcid.org/0000-0002-2709-4321.

References

ASME 2009 Surface texture (surface roughness, waviness, and lay). *Revision of ANSI/ASME* B46.1-1995. Standard. ASME.

Barros, J.M., Schultz, M.P. & Flack, K.A. 2018 Measurements of skin-friction of systematically generated surface roughness. *Intl J. Heat Fluid Flow* **72**, 1–7.

Bons, J.P. 2002 S_t and C_f augmentation for real turbine roughness with elevated freestream turbulence. *J. Turbomach.* **124** (4), 632–644.

Busse, A., Thakkar, M. & Sandham, N.D. 2017 Reynolds-number dependence of the near-wall flow over irregular rough surfaces. *J. Fluid Mech.* **810**, 196–224.

Chin, C.C., Hutchins, N., Ooi, A.S.H. & Marusic, I. 2009 Use of direct numerical simulation (DNS) data to investigate spatial resolution issues in measurements of wall-bounded turbulence. *Meas. Sci. Technol.* **20**, 115401.

Clauser, F.H. 1956 The turbulent boundary layer. *Adv. Appl. Mech.* **4**, 1–51.

Djenidi, L., Talluru, K.M. & Antonia, R.A. 2018 Can a turbulent boundary layer become independent of the Reynolds number? *J. Fluid Mech.* **851**, 1–22.

Djenidi, L., Talluru, K.M. & Antonia, R.A. 2019 A velocity defect chart method for estimating the friction velocity in turbulent boundary layers. *Fluid Dyn. Res.* **51**, 045502.

Flack, K.A., Schultz, M.P. & Barros, J.M. 2020 Skin friction measurements of systematically-varied roughness: probing the role of roughness amplitude and skewness. *Flow Turbul. Combust.* **104** (2), 317–329.

Flack, K.A., Schultz, M.P., Barros, J.M. & Kim, Y.C. 2016 Skin-friction behavior in the transitionally-rough regime. *Intl J. Heat Fluid Flow* **61**, 21–30.

Forooghi, P., Stroh, A., Magagnato, F., Jakirlić, S. & Frohnapfel, B. 2017 Toward a universal roughness correlation. *J. Fluids Engng* **139** (12), 121201.

Furuya, Y., Miyata, M. & Fujita, H. 1976 Turbulent boundary layer and flow resistance on plates roughened by wires. *J. Fluids Engng* **98** (4), 635–643.

Hama, F.R. 1954 Boundary layer characteristics for smooth and rough surfaces. *Trans. Soc. Nav. Archit. Mar. Engrs* **62**, 333–358.

Hutchins, N., Nickels, T.B., Marusic, I. & Chong, M.S. 2009 Hot-wire spatial resolution issues in wall-bounded turbulence. *J. Fluid Mech.* **635**, 103–136.

Jiménez, J. 2004 Turbulent flows over rough walls. *Annu. Rev. Fluid Mech.* **36**, 173–196.

Kamruzzaman, M.D., Djenidi, L., Antonia, R.A. & Talluru, K.M. 2015 Drag of a turbulent boundary layer with transverse 2D circular rods on the wall. *Exp. Fluids* **56** (6), 121.

Krogstad, P.-Å. & Antonia, R.A. 1999 Surface roughness effects in turbulent boundary layers. *Exp. Fluids* **27** (5), 450–460.

Krogstad, P.-Å. & Efros, V. 2012 About turbulence statistics in the outer part of a boundary layer developing over two-dimensional surface roughness. *Phys. Fluids* **24**, 075112.

Leonardi, S., Orlandi, P., Djenidi, L. & Antonia, R.A. 2015 Heat transfer in a turbulent channel flow with square bars or circular rods on one wall. *J. Fluid Mech.* **776**, 512–530.

Leonardi, S., Orlandi, P., Smalley, R.J., Djenidi, L. & Antonia, R.A. 2003 Direct numerical simulations of turbulent channel flow with transverse square bars on one wall. *J. Fluid Mech.* **491**, 229–238.

https://doi.org/10.1017/jfm.2022.242 Published online by Cambridge University Press

LIGRANI, P.M. & BRADSHAW, P. 1987 Spatial resolution and measurement of turbulence in the viscous sublayer using subminiature hot-wire probes. *Exp. Fluids* **5** (6), 407–417.

MACDONALD, M., CHAN, L., CHUNG, D., HUTCHINS, N. & OOI, A. 2016 Turbulent flow over transitionally rough surfaces with varying roughness densities. *J. Fluid Mech.* **804**, 130–161.

MARUSIC, I., CHAUHAN, K.A., KULANDAIVELU, V. & HUTCHINS, N. 2015 Evolution of zero-pressure-gradient boundary layers from different tripping conditions. *J. Fluid Mech.* **783**, 379–411.

MARUSIC, I., MONTY, J.P., HULTMARK, M. & SMITS, A.J. 2013 On the logarithmic region in wall turbulence. *J. Fluid Mech.* **716**, R3.

MUSKER, A.J. 1980 Universal roughness functions for naturally-occurring surfaces. *Trans. Can. Soc. Mech. Engng* **6** (1), 1–6.

NAPOLI, E., ARMENIO, V. & DE MARCHIS, M. 2008 The effect of the slope of irregularly distributed roughness elements on turbulent wall-bounded flows. *J. Fluid Mech.* **613**, 385–394.

NICKELS, T.B., MARUSIC, I., HAFEZ, S. & CHONG, M.S. 2005 Evidence of the k_1^{-1} law in a high-Reynolds-number turbulent boundary layer. *Phys. Rev. Lett.* **95**, 074501.

NIKURADSE, J. 1933 Laws of flow in rough pipes. *Translation from German published 1950 as NACA Tech. Memo* 1292.

PERRY, A.E. & JOUBERT, P.N. 1963 Rough-wall boundary layers in adverse pressure gradients. *J. Fluid Mech.* **17** (02), 193–211.

PERRY, A.E. & LI, J.D. 1990 Experimental support for the attached-eddy hypothesis in zero-pressure-gradient turbulent boundary layers. *J. Fluid Mech.* **218**, 405–438.

PLACIDI, M. & GANAPATHISUBRAMANI, B. 2015 Effects of frontal and plan solidities on aerodynamic parameters and the roughness sublayer in turbulent boundary layers. *J. Fluid Mech.* **782**, 541–566.

SCHLATTER, P. & ÖRLÜ, R. 2010 Assessment of direct numerical simulation data of turbulent boundary layers. *J. Fluid Mech.* **659**, 116–126.

SCHLICHTING, H. & KESTIN, J. 1961 *Boundary Layer Theory*, vol. 121. Springer.

SCHULTZ, M.P. & FLACK, K.A. 2007 The rough-wall turbulent boundary layer from the hydraulically smooth to the fully rough regime. *J. Fluid Mech.* **580**, 381–405.

SCHULTZ, M.P. & FLACK, K.A. 2009 Turbulent boundary layers on a systematically varied rough wall. *Phys. Fluids* **21**, 015104.

SILLERO, J.A., JIMÉNEZ, J. & MOSER, R.D. 2014 Two-point statistics for turbulent boundary layers and channels at Reynolds numbers up to $\delta^+ = 2000$. *Phys. Fluids* **26**, 105109.

SQUIRE, D.T., MORRILL-WINTER, C., HUTCHINS, N., SCHULTZ, M.P., KLEWICKI, J.C. & MARUSIC, I. 2016 Comparison of turbulent boundary layers over smooth and rough surfaces up to high Reynolds numbers. *J. Fluid Mech.* **795**, 210–240.

SUN, B. 2019 Thirty years of turbulence study in China. *Appl. Math. Mech.* **40** (2), 193–214.

WAIGH, D.R. & KIND, R.J. 1998 Improved aerodynamic characterization of regular three-dimensional roughness. *AIAA J.* **36** (6), 1117–1119.

https://doi.org/10.1017/jfm.2022.242 Published online by Cambridge University Press